Check for updates

Novel MOF grown on Ni foam as an *ex situ* absorptive medium for the remediation of Hg polluted water in surface water

E. Yosef, M. Halanur, (iD) D. Levy and H. Mamane (iD) *

A novel metal organic framework (MOF) was fabricated on the surface of an open cell nickel foam and employed as a selective sorbent for Hg^{2+} dissolved in surface water. Two organic ligands (2-amino-teraphthalate and 4,4-dipyridyl) were combined with $Ni(NO_3)_2$ and grown on a Ni foam (95% porosity) to generate a $P4_1$ symmetric MOF with an internal 2.487 Å pore size and an active amino moiety serving as a binding site for Hg^{2+} and other heavy metals, characterized by XRD, and a lenticular crystal habit producing relatively well distributed spherical crystals, characterized by SEM-EDX. Adsorption experiments were conducted in both deionized water and mercury spiked into river water at concentrations typical for polluted areas ([Hg^{2+}] ~ 4, 40, and 400 ppb). The adsorption effect was characterized by Au-stabilized ICP-MS, finding highly favorable adsorptive efficacy, exhibiting adsorption capacities of 201.31 mg g^{-1}, 25.68 mg g^{-1}, and 3.017 mg g^{-1}, at initial concentrations of 400 ppb, 40 ppb, and 4 ppb, respectively. The coating of the MOF on the metal foam modulated the adsorption behavior of the MOF, maximizing the effective surface area of the adsorbent and thereby reversing the otherwise inverse relationship of % adsorbed with respect to increasing C_i.

Water impact

A novel metal–organic framework (MOF) coated on open-cell nickel foam was developed as a selective sorbent for Hg^{2+} in surface water, achieving high adsorption capacities at low concentrations. This paper demonstrates a new platform: MOF@foam, that can maximize the adsorptive capacities of MOFs compared to their powdered form. By exploiting this platform, and the benefits of hierarchical porosity that it confers, other MOFs may be developed to adsorb a large range of other persistent pollutants.

1. Introduction

Mercury (Hg), like other heavy metal pollutants, has been studied extensively both as a highly dangerous and persistent pollutant and as a target for adsorption by functional absorptive materials.[1] The challenge of removing Hg from polluted water sources is particularly difficult, given its ability to produce ecocidal effects even at extremely low concentrations,[2] the high concentration of other water constituents within polluted water, and the large volume of such water. Currently, there is no technology available that is efficient, selective, and cost-effective enough to absorb and remove mercury from polluted water, which realistically present Hg concentrations in the low ppb range.[3] Metal organic frameworks (MOFs) have emerged as an attractive route to such a technology,[4–6] with absorptive capacities (Q_e) of some MOF materials reported as high as 0.0451 mg g^{-1},

even when the initial concentration (C_i) is as low at an initial concentration (C_i) of 12 ppb.[7] Other previously reported MOF materials are listed in Table 1, where Q_e values are shown for the lowest C_i tested, given the proportional relationship between C_i and Q_e.

The internal porosity of MOF materials and the selective binding of moieties within the ligand structure, provide the basis for the highly effective absorption of particularly challenging pollutants like Hg. However, either the lack of any mesoporous or macroporous structural elements or the hydrophobicity of MOF surfaces, or more likely a combination of these factors, produce significant limits on Q_e for powdered MOF materials. This problem is compounded in real surface water, rarely the subject of MOF absorption studies, where powdered MOF materials become fouled by otherwise common water constituents long before its ideal adsorptive capacity can even be reached.

Thus, a need exists to integrate MOF materials, and indeed other classes of adsorbents, with durable mesoporous or macroporous scaffolds to investigate the joint effect. Similar

School of Mechanical Engineering, Faculty of Engineering, Tel Aviv University, Tel Aviv 69978, Israel. E-mail: hadasmg@tauex.tau.ac.il

This journal is © The Royal Society of Chemistry 2025

Environ. Sci.: Water Res. Technol., 2025, **11**, 2747–2754 | 2747

Table 1 Comparison of Hg-adsorbent MOFs in the field

Material	Q_e at min. C_i (mg g^{-1})	Minimum C_i ([Hg] = ppb)	Time (minute)	References
BioMOF	2.0500	10 000	10 080	8
Thiol-HKUST-1	0.008	8.1	1440	9
Zn(hip)(L)·(DMF)(H$_2$O)	1.620	100	60	10
DUT-67	0.045	12	n/a	7
This work	0.003	4	60	

methods are already employed in the fabrication of permeable reactive barriers (PRBs), a class of technologies used for the *in situ* mitigation of damage to groundwater supplies from known contamination plumes underground.[11] PRBs are installed in the groundwater flow direction, and their permeability allows for water to pass through and dissolved contaminants to react with a PRB reactive surface. A similar method is also applied in the nano-selenium coating applied to the inner surface of a polyurethane foam, with exceptional results, albeit with expensive and fragile materials.[12]

The same durability beneficial to metal foam materials' application as PRB could serve well as an application as a scaffolding for an *ex situ* reactive medium. Many types of foams are commercially available, and their surface chemistry can be easily modified by various methods for affixation of high performance sorbents for Hg. Much of the development of materials engineering of functional coatings on metal foams has been conducted in the electrochemical field, where various MOFs have been fabricated on metal foam materials for applications as electrical components.[13,14] The goal of the present study is to apply a MOF material grown selectively on the internal surface of a metal foam for the effective treatment of Hg contamination in realistic concentrations.

2. Materials and methods

95% porosity open-cell Ni foam was sourced from Recemat, delivered from the Netherlands. 2-Amino-teraphthalate, 4,4-dipyridyl, Zn(NO$_3$)$_2$·6H$_2$O reagent grade 98, and dimethyl formamide (DMF) solvent were obtained from Sigma-Aldrich.

2.1. MOF@foam synthesis

For each MOF@foam sample, 2-amino-teraphthalate (0.050 g), 4,4-dipyridyl (0.043 g), and Zn(NO$_3$)$_2$·6H$_2$O (0.083 g) were mixed with 20 mL of DMF : ddH$_2$O (5 : 1) in a PTFE thermal reactor. Separately, circular pieces of Ni foam (diameter = 30 mm, height = 1.6 mm) with an average weight of 0.486 g were sonicated for 10 minutes in 1% HCl, then cleaned and sonicated with ddH$_2$O, until the cleaning solution registered a neutral pH. The foam was then added to the thermal reactor with the other reactants, and heated to 120 °C for 40 hours, then left to cool. The resultant MOF@foam composite was washed three times with 100 mL DMF, removing excess MOF material, then three times with 200 mL ddH$_2$O, then dried overnight at 60 °C, producing a MOF coating with an average mass of 39.5 mg over foams

having an average 642 mg. The chemical formula of the resultant MOF coating was Zn(C$_{10}$H$_8$N$_2$)(C$_8$H$_5$NO$_4$).

2.2. Powder MOF synthesis

An identical MOF was synthesized without the Ni foam substrate, wherein 2-amino-teraphthalate (0.05 g 2.8 mmol), 4,4-dipyridyl (0.043 g, 2.8 mmol) and Zn(NO$_3$)$_2$·6H$_2$O (0.083 g, 2.8 mmol as Zn) were mixed with 5 mL of DMF : ddH$_2$O (5 : 1) in a PTFE thermal reactor and heated to 120 °C for 40 hours, then left to cool. The resultant powder was washed with DMF, then ddH$_2$O, then dried overnight at 60 °C, producing a yellow MOF.

2.3. Absorption experiments

Absorption of Hg was conducted in surface water collected from the Yarkon River in Tel Aviv and filtered with 0.45 μm membrane (from Millipore), then spiked with HgCl$_2$ to produce solutions of ~[Hg]: 400; 40; and 4 ppb. Other water quality parameters for the Yarkon River water were characterized by with a MRC-103 multiparameter probe, finding a conductivity of 1268 mS, a pH of 6.7, ORP of 183 mV, and calculating a hardness of 761 ppm equ. CaCO$_3$. Absorption experiments were also conducted in Hg in ddH$_2$O for comparison, and further in ddH$_2$O containing similar concentrations of Hg, Cd, and Pb, to assess for selectivity. All [Hg] results were obtained with an Agilent 7500 ICP MS at Tel Aviv University, and all samples were made up to 2% HCl and 5% HNO$_3$ using ultrapure materials from Sigma Aldrich and were additionally stabilized with 1 ppm of Au from Sigma Aldrich Au ICP standard.

The Hg uptake, q_t (mg g^{-1}), which is the amount of adsorbed Hg at time t (min) on a specific amount of MOF@foam, was determined using the following equation:

$$q_t = \frac{(C_i - C_t) \cdot V}{m} \tag{1}$$

where C_i and C_t (mg g^{-1}) are the initial Hg concentration and the concentration at time t, respectively, V (L) is the volume of the solution, and m (g) is the dose of the adsorbent MOF material, which was derived from the mass difference between the composite and the raw unmodified foam. The percentage of Hg removal was calculated using the following equation:

$$\text{Hg removal \%} = \frac{C_i - C_t}{C_i} \cdot 100\% \tag{2}$$

Batch experiments were conducted in 50 mL volumes of

2748 | *Environ. Sci.: Water Res. Technol.*, 2025, **11**, 2747–2754

This journal is © The Royal Society of Chemistry 2025

Hg-containing solutions agitated at room temperature in a mechanical shaker incubator at 150 rpm. Sample volumes were passed through a 0.45 μm filter to remove any loose MOF particles, then diluted with a stabilization solution for ICP analysis.

Adsorption kinetics. Two linear forms of kinetic models were examined for the MOF@foam. The first model is the pseudo-first-order equation of Lagergren for the sorption of a liquid/solid system based on the solid capacity, which is the most widely used expression for liquid-phase sorption processes, and can be represented as follows:

$$\log(q_e - q_t) = -\frac{k_1 t}{2.303} + \log q_e \quad (3)$$

where q_e (mg g^{-1}) is the amount of Hg adsorbed per unit mass of MOF at equilibrium, and k_1 (min^{-1}) is the rate constant of the pseudo-first-order model. This model can also be expressed as the differential eqn (4) and then integrated into the linear eqn (5).

$$\frac{\delta q_t}{\delta t} = k_t(q_e - q_t) \quad (4)$$

$$\frac{1}{k_1} \cdot \ln(q_e - q_t) = t \quad (5)$$

The second model is the Lagergren pseudo-second-order equation, expressed in the linear form (6):

$$\frac{t}{q_t} = \frac{t}{q_e} + \frac{1}{k_2 q_e^2} \quad (6)$$

where, k_2 (g mg^{-1} min^{-1}) represents the rate of the pseudo-second-order model.

2.4. Characterization

Scanning Electron Microscopy (SEM) was conducted with a Thermo Fisher Quanta 200 FEG ESEM instrument, which employs energy-dispersive X-ray spectroscopy (EDS). Crystallinity was analyzed using powder X-ray diffraction (Empyrean II Diffractometer) operating with Cu-Kα$_1$ radiation (l = 1.54 Å) at a scan rate of 3° min^{-1} and a 2 theta range of 5–80°, using mercury software for analysis, and comparing to other known MOF crystal structures. Zeta potential was measured by an Anton Paar, SurPASS 3 instrument using 0.001 M KCl, where streaming potential measurements were conducted at pH 7.

3. Results and discussion

3.1. Materials characterization

SEM characterization demonstrates several features of the composite material and its fabrication method, including that the MOF coating is well distributed within the inner surface of the metal foam, as shown in Fig. 1A.

The foam is pre-treated with 1% HCl which likely activates the foam's surface for nucleation. Then, MOF is immobilized on the foam by selectively growing the MOF crystals on the internal surface of the Ni foam during the synthesis process.
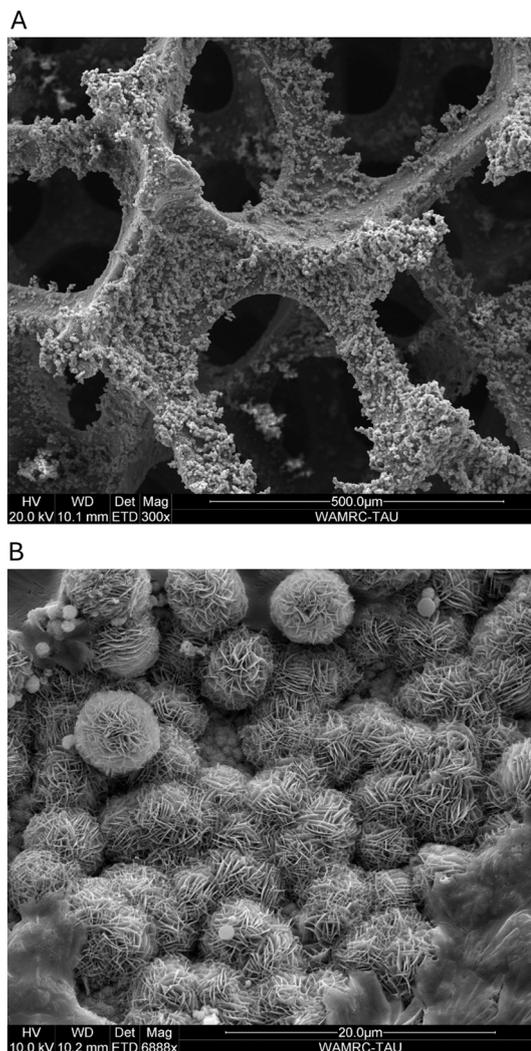

Fig. 1 A: Scanning electron micrograph of MOF@foam coating. B: Scanning electron micrograph of MOF@foam crystal structure.

The forces keeping the MOF attached to the foam include chemical bonding between the MOF and the Ni foam surface, as well as physical adhesion due to rough surface itself. The MOF crystals preferentially crystallize on the Ni foam's surface rather than forming free-floating particles, ensuring effective immobilization and the selective crystallization ensures a strong interaction between the MOF and the foam substrate.

Whilst the deposition of the MOF on the metal foam may not generate a nanometrially uniform layer throughout the complex internal geometry, the selectivity of MOF

Table 2 Elemental distribution derived from EDS

Element	Wt%	Wt% sigma	Atomic%	Theoretical atomic% for MOF
C	41.44	0.69	63.05	69.12
O	22.80	0.50	26.05	20.48
Zn	7.18	0.39	2.01	10.4
Ni	28.57	0.50	8.89	*Not relevant*

This journal is © The Royal Society of Chemistry 2025

Environ. Sci.: Water Res. Technol., 2025, **11**, 2747–2754 | **2749**

crystallization for the metal foam surface over existing MOF surfaces ensures the effective (exposed) surface area of the MOF material is significantly higher than for undeposited MOF material, raising its potential for adsorptive effects.

The MOF crystals themselves display, at the micrometric level, a lenticular crystal habit that generates sphere-like crystals each containing a high density of internal porosity, as shown in Fig. 1B. This microstructural porosity also provides ample opportunity for adsorbates in solution to penetrate within the MOF, further enhancing the potential for adsorption. The combination of macrometric, mesometric, micometric, and nanometric porosities, provides a hierachical porosity that allows the MOF material greater capitalization of its adsorption capacity.
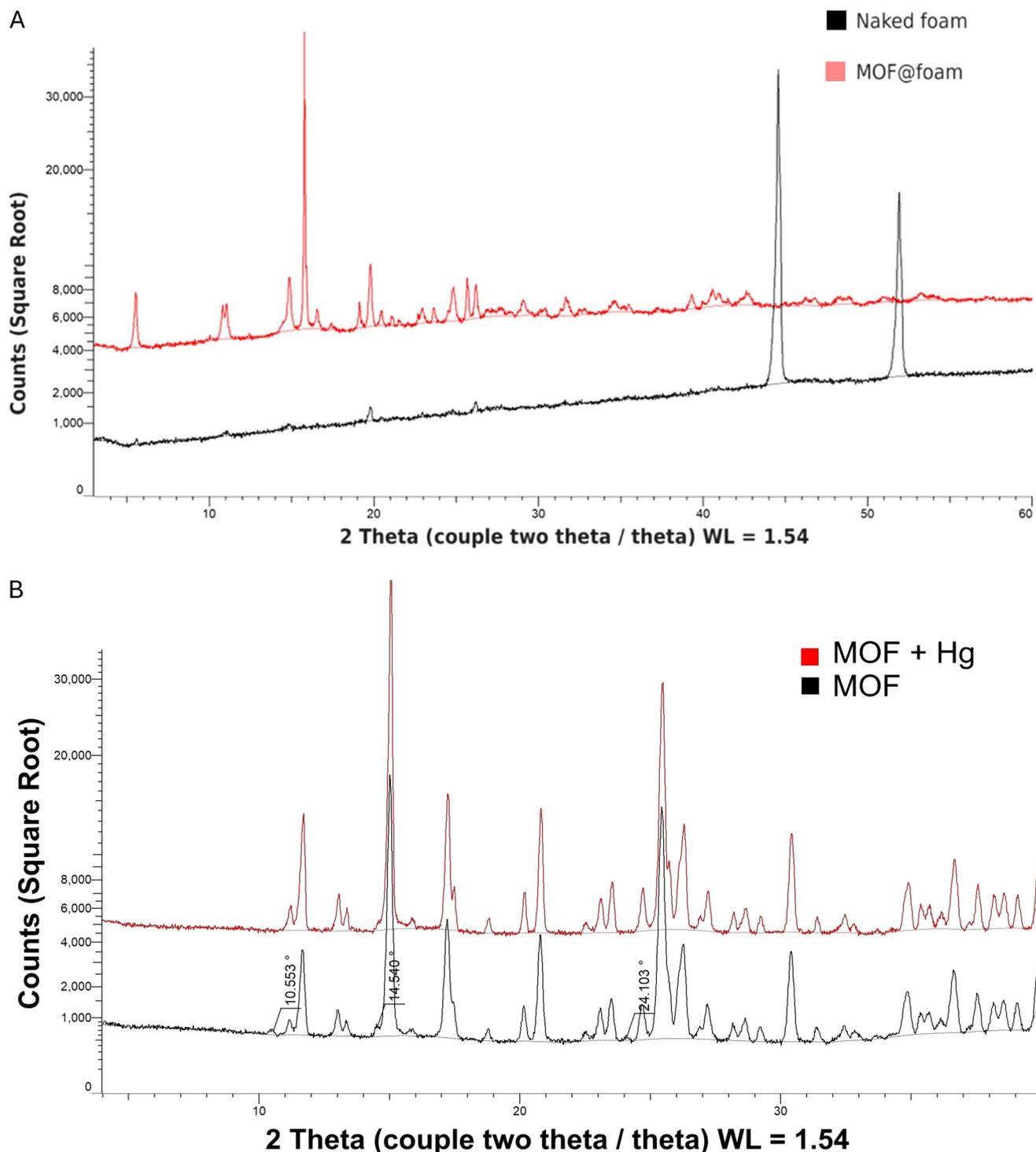
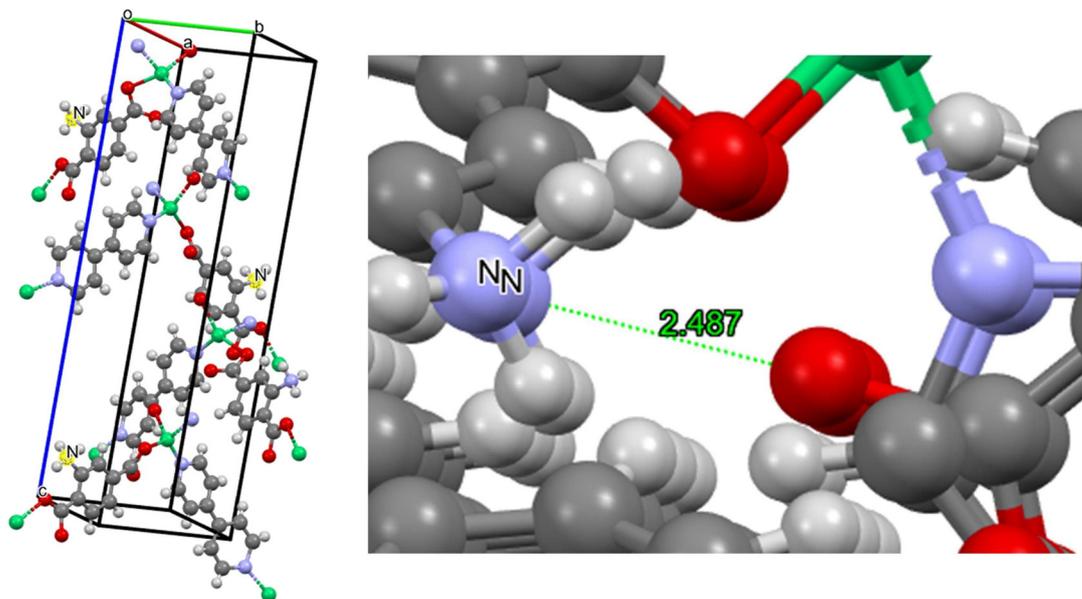Fig. 2   XRD spectrum of $P4_1$ MOF@foam before (A) and after (B).

Fig. 3 Resolved crystal structure and pore geometry of $P4_1$ MOF.

EDS measurements coupled with the scanning electron micrographs indicate the stoichiometric ratio of elements contained within the MOF@foam composite surface correlates to the theoretical molecular structure of the MOF material.

Energy-dispersive X-ray spectroscopy results shown in Table 2 indicate a close approximation of theoretical values for the composition of the MOF material. Depositing the MOF on a Ni foam produces some obscuring effects, most notably that the K-beta line of Ni (8.26 keV) is close to that K-alpha line of zinc (8.64 keV), thus zinc may be underdetected in the EDS. The underdetection of light elements such as N in low concentrations may explain why N is not detected in the EDS spectrum.

A resolution of the PXRD results of the MOF indicated a $P4_1$ structure, with a major peak at approximately 16°, indicative of a key crystalline facet in its tetragonal symmetry. Additional minor peaks at 5.5°, 11° (a double peak), 15°, 20°, 25°, and 26° suggest a complex lattice structure typical of MOF materials. The simulated PXRD pattern derived from the resolved CIF structure ($P4_1$ space group; a = 15.21 Å, c = 7.88 Å) aligns well with the experimental PXRD data. Notably, the intense peak 14.5° corresponds to the (0 1 0) reflection with a d-spacing of 7.88 Å, consistent with tetragonal symmetry and characteristic of MOFs adopting $P4_1$-type frameworks. As shwon in Fig. 2, the PXRD spectra before and after Hg adsorption remain identical, indicating that the crystal structure of the MOF framework was retained. This stability suggests that Hg adsorption occurs through localized interactions – likely at the amino functional groups – without inducing significant structural rearrangement detectable by powder diffraction.

Following resolution of the crystal structure form XRD data, $P4_1$ tetragonal geometry was identified, and the size of the pore in was calculated to be 2.487 Å, wherein both sides

of the pore are adjacent to a nitrogen atoms in amide moieties able to coordinate and bind Hg^{2+}, among other divalent cations. The atomic sizes of Hg^{2+}, Hg^{1+}, and Hg^0, all of which exist as stable species in surface water containing other salts and organic matter, are 1.10 Å, 1.25 Å, and 1.55 Å, respectively, and thus the 2.487 Å is sufficient for Hg-binding. In Fig. 3: dark grey represents carbon, light grey represents hydrogen; red represents oxygen; green represents nickel; and blue represents nitrogen.

3.2. Surface charge of MOF@foam

The addition of the MOF coating on the Ni foam produces a greater negative surface charge, attributable to the presence of the carboxylic acid groups of the coordinating groups in the 2-amino-teraphthalate ligands, which can be seen in
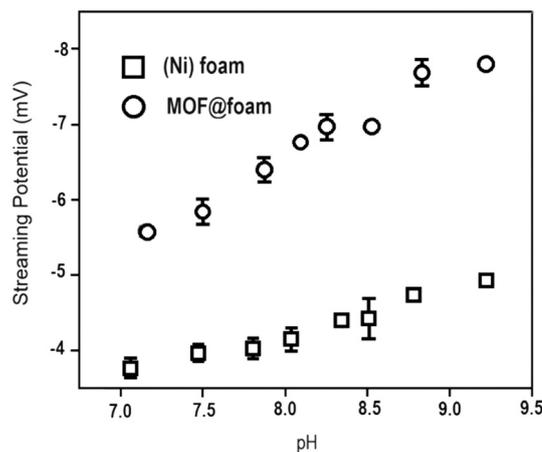

Fig. 4 Zeta of MOF@foam *vs.* foam.

Fig. 4. This extra negative surface charge, even on the mV scale, likely aids the adsorption of cations like Hg.

3.3. Adsorption of Hg by the MOF and MOF@foam composite

Overviews of the adsorptions of Hg by the MOF@foam composites at three different concentrations ($\sim$4 ppb, $\sim$40 ppb, $\sim$400 ppb) were conducted in triplicate, and analysed with respect to time, reaching a maximum q_t at 1 hour. The adsorption kinetics of the MOF@foam composite were found to adhere to a pseudo 2nd order kinetic model, with the exception of initial period of adsorption at the lowest range tested ([Hg] $\sim$ 4 ppb), see Table 3. This indicates that at lower concentrations the physi-sorptive effect is more pronounced than the chemi-sorptive effect, which is consistent with both the highly nano, micro, and microporous structure of the MOF@foam composite and the relatively low affinity of the amide group for Hg, when compared to thiol groups or precious metal nanoparticles. Analysis for Zn was also undertaken to determine leaching into the samples from the MOF coating, finding negligible change in concentration, indicating that loose MOF coating was removed during the washing step of the fabrication.

The initial adsorption (up to t = 45 minutes) in filtered freshwater fits very closely to the pseudo first order kinetic model, demonstrating an R-value much higher than that for all data points, indicating a lack of competition of Hg^{2+} for amide active sites in the MOF@foam, crucial for practical application. After this initial period the adsorption relationship becomes more chemi-sorptive in character, due to competition for the active sites, a relationship maintained at higher concentrations, see Table 3.

Due to the proportional relationship between C_i and q_t values, q_t (and q_e) values for many adsorbents at the low concentrations realistically found in contaminated surface water are in the µg g^{-1} range.[3] This work found that at [Hg] $\sim$ 4 ppb, the range of likely sorption capacities is between 200 and 350 µg g^{-1}, with equilibrium typically reached within 1 hour, as shown in Fig. 5a. For higher initial concentrations of 40 ppb and 400 ppb, the adsorption capacities were found in a range of 1.6 to 2.6 mg g^{-1} and 32 mg g^{-1} to 38 mg g^{-1}, as shown in Fig. 5b and c, respectively.
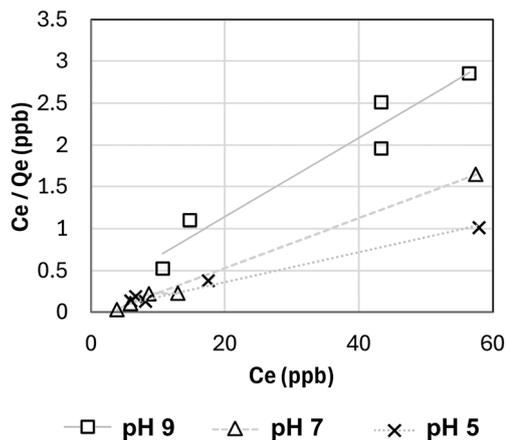

Fig. 5 Langmuir isotherm for adsorption of Hg by MOF@foam in ddH$_2$O at three different pH values.

The very high q_t values – given the initial concentrations – displayed by the MOF coating on the metal foam are facilitated by the maximization of exposure of the MOF to the influent fluid and minimizing the mass of MOF actually used for adsorption.

The deposition of the MOF material on the internal surface of the Ni foam modulates the relationship between the MOF's adsorptive effect and the initial concentration, to produce a logarithmic correlation indicating that the effective surface area of non-deposited MOF material represents a limitation to % Hg removal that is effectively overcome by deposition on the surface. Lower % Hg removals at lower initial concentrations for the MOF@foam composite in Fig. 6 are likely due to the batch adsorption nature of the experiment: without a means of forcing the solution through the internal geometry of the composite, flow effects produce a limiting factor on the extent of penetration and thus of adsorption.

Maintaining the metal foam material – which constitutes the most cost-prohibitive aspect of the MOF@foam composite – is paramount for sustainability, and thus the used composite material was stripped under 5% HCl and sonication for 60 minutes, then redeposited with the MOF material using the same hydrothermal deposition procedure described in the Materials and Methods section. The resultant MOF coating can then be used for Hg batch

Table 3 Kinetic models of Hg batch adsorption

Parameter		[Hg] $\sim$ 4 ppb	[Hg] $\sim$ 40 ppb	[Hg] $\sim$ 400 ppb
$q_e^{experimental}$ (µg g^{-1})		3.017	25.68	201.31
Pseudo 1st order	$q_e^{calculated}$ (µg g^{-1})	2.289	20.81	186.42
	Δq (%)	24.1%	19%	7.4%
	R^2	0.905	0.883	0.891
	k_1 (min^{-1})	0.126	0.0408	0.166
Pseudo 2nd order	$q_e^{calculated}$ (µg g^{-1})	3.215	28.21	215.67
	Δq (%)	6.56%	9.86%	7.13%
	R^2	0.929	0.994	0.996
	k_2 (min^{-1})	0.00331	0.00221	0.000223

2752 | *Environ. Sci.: Water Res. Technol.*, 2025, **11**, 2747–2754

This journal is © The Royal Society of Chemistry 2025
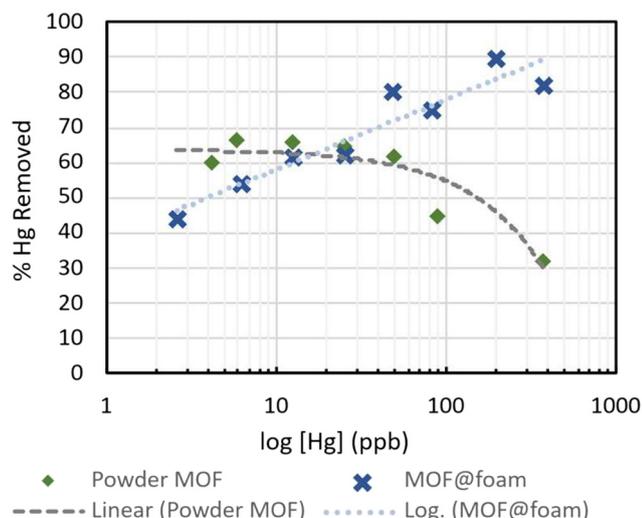
Fig. 6 % removed of MOF@foam vs. naked MOF at different C_i.

Fig. 8 Adsorption of other heavy metal ions.

consistent with both the highly nano, micro, and microporous structure of the MOF@foam composite and the relatively low affinity of the amide group for Hg, when compared to thiol groups or precious metal nanoparticles.

Batch adsorption was also carried out with ddH$_2$O in which both Cd and Pb were also dissolved, all at 100 ppb, at three pH levels (5, 7, and 9), finding slight favorability for Hg over Cd and Pb, as shown in Fig. 8. The MOF coating shows increasing adsorption of Hg as pH decreases, owing to the enhanced protonation of amino functional groups at lower pH, facilitating electrostatic attraction of Hg species. The adsorption of Cd shows the opposite behavior due to the increased formation and availability of negatively charged Cd hydroxide complexes at higher pH, enhancing electrostatic interactions. Adsorption of Pb by the MOF reaches a minimum at neutral pH and significantly higher levels at both acidic and basic conditions, likely due to competitive formation of different Pb species at varying pH conditions, promoting adsorption through either electrostatic attraction at acidic pH or precipitation and surface complexation at basic pH. In practical application, marine water limits the adsorption of Hg more than competing heavy metal cations, as seen in Fig. 9.

adsorption, the results of which are shown in Fig. 7. In order to account for the differences in C_i in the experimental procedure, Fig. 7 is shown with partition coefficient, which is equivalent to $(Q_e/C_e) \cdot V_{exp}$, which provides a measure of the adsorptive effect independent of initial concentration, allowing for comparisons. As can be seen, with the exception of the higher concentration, the MOF@foam material demonstrated broadly consistent adsorptive effects through multiple cycles, indicating that neither the deposition or removal process affects the surface of the metal foam in a way that compromises the adsorptive relationship between the MOF and the Hg, as seen in Fig. 7.

The kinetics of adsorption for Hg by the MOF@foam varies consistently with initial concentration, demonstrating a closer fit to a pseudo first order kinetic model at lower concentrations and a closer fit to a pseudo second order kinetic model at higher concentrations. This indicates that at lower concentrations the physi-sorptive effect is more pronounced than the chemi-sorptive effect, which is
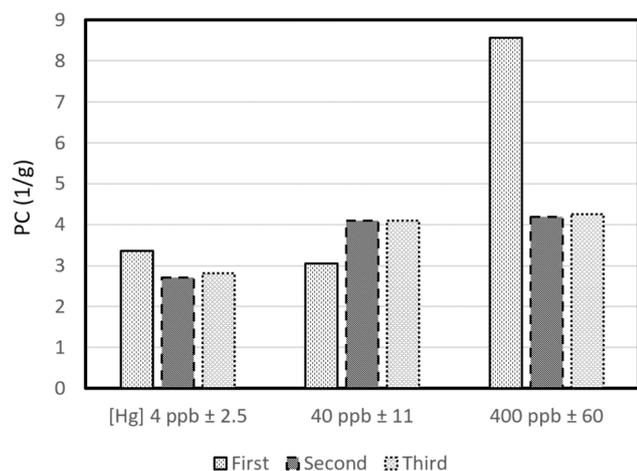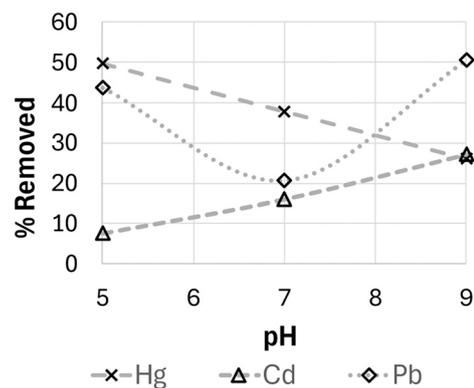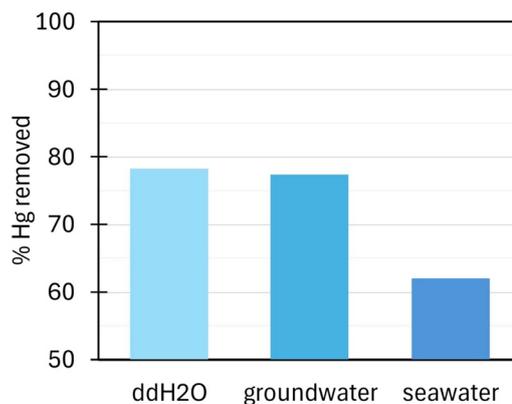

Fig. 7 Cycle efficiency for Hg removal.

Fig. 9 Comparative percentage adsorption of Hg by MOF@foam at [Hg] = 100 ppb in three different water types.

This journal is © The Royal Society of Chemistry 2025

Environ. Sci.: Water Res. Technol., 2025, 11, 2747–2754 | 2753

4. Conclusion

Coating the MOF material on the internal surface of the foam produced a durable MOF@foam composite with enhanced adsorption characteristics, maintaining pseudo 1st order kinetics at very low concentrations (<40 ppb) and pseudo 2nd order kinetics at higher concentrations still within the ppb range. In this study, Hg is an example of possible adsorbate present in low concentrations in high matrix water, such as the freshwater, wherein the designed $P4_1$ dual-ligand Zn-MOF's adsorption was improved by coating on a foam. This MOF@foam platform can therefore be applied to a number of other MOF systems, by appropriately activating the surface of the foam to form a nucleating surface, and lowering the concentration of reactants in the synthesis to produce preferential crystallization thereon. Utilization of such a MOF@foam platform should investigate the electro-sorptive applications, wherein the metal foam conductivity is leveraged to enhance selectivity and kinetics with fine control of the surface voltage.

Author contributions

Eitan Yosef executed the research and wrote the manuscript, Dr. Manohara Halanur assisted with fabrication, characterization, and kinetic analysis. Dr. Davide Levy performed the XRD analysis and provided and resolved a crystal structure therefrom. As principal investigator, Professor Hadas Mamane organized, directed, and provided executive advice and direction on the research.

Conflicts of interest

There are no conflicts to declare.

Data availability

Data relating to the above paper is available on request, including the raw .csv files provided by the ICP-MS machine, as well as other raw files produced by other characterization techniques. The process and product of the mathematical analysis conducted on said raw data is available in the body of the above paper, but – if so requested – can be provided in Excel format.

Acknowledgements

References

1 J. G. Yu, B. Y. Yue and X. W. Wu, *et al.*, *Environ. Sci. Pollut. Res.*, 2016, **23**, 5056–5076, DOI: **10.1007/s11356-015-5782-7**.

2 D. W. Boening, *Chemosphere*, 2000, **40**, 1335–1351, DOI: **10.1016/S0045-6535(99)00346-4**.

3 V. Kumar, A. Sharma, R. Kumar, R. Bhardwaj, A. K. Thukral and J. Rodrigo-Comino, *Hum. Ecol. Risk Assess.*, 2020, **26**, 1–16, DOI: **10.1080/10807039.2018.1553610**.

4 P. A. Kobielska, *Coord. Chem. Rev.*, 2018, **358**, 92–107, DOI: **10.1016/j.ccr.2017.12.001**.

5 G. R. Xu, Z. H. An, K. Xu, Q. Liu, R. Das and H. L. Zhao, *Coord. Chem. Rev.*, 2021, **427**, 213554, DOI: **10.1016/j.ccr.2020.213554**.

6 F. Zadehahmadi, N. T. Eden, H. Mahdavi, K. Konstas, J. I. Mardel, M. Shaibani, P. C. Banerjee and M. R. Hill, *Env. Sci.: Water Res. Technol.*, 2023, **9**, 1305.

7 S. Chen, F. Feng, S. Li, X.-X. Li and L. Shu, *Chem. Speciation Bioavailability*, 2018, **30**, 106–199, DOI: **10.1080/09542299.2018.1463832**.

8 M. Mon, F. Lloret, J. Ferrando-Soria, C. Martí-Gastaldo, D. Armentano and E. Pardo, *Angew. Chem., Int. Ed.*, 2016, **55**, 11167–11172, DOI: **10.1002/anie.201606572**.

9 K. Fei, *et al.*, *J. Hazard. Mater.*, 2011, **196**, 36–43, DOI: **10.1016/j.jhazmat.2011.08.087**.

10 J. Zhou, H. Zhang, T. Xie, Y. Liu, Q. Shen, J. Yang, L. Cao and J. Yang, *J. Environ. Sci.*, 2022, **119**, 33–43, DOI: **10.1016/j.jes.2021.06.004**.

11 J. Song, G. Huang, D. Han, Q. Hou, L. Gan and M. Zhang, *J. Cleaner Prod.*, 2021, **319**, 128644, DOI: **10.1016/j.jclepro.2021.128644**.

12 S. Ahmed, J. Brockgreitens, K. Xu and A. Abbas, *Adv. Funct. Mater.*, 2017, **27**, 1606572, DOI: **10.1002/adfm.201606572**.

13 K. Huang, S. Guo, R. Wang, S. Lin, N. Hussain, H. Wei, B. Deng, Y. Long, M. Lei, H. Tang and H. Wu, *Chin. J. Catal.*, 2020, **41**, 1754–1760, DOI: **10.1016/S1872-2067(20)63510-4**.

14 G. Zhi, X. Qi, Y. Li, J. Wang and J. Wang, *Sep. Purif. Technol.*, 2024, **328**, 124927, DOI: **10.1016/j.seppur.2023.124927**.

2754 | *Environ. Sci.: Water Res. Technol.*, 2025, **11**, 2747–2754

This journal is © The Royal Society of Chemistry 2025